Published in final edited form as:
Electrophoresis. 2012 September ; 33(17): 2718–2724. doi:10.1002/elps.201200069.

High Electric Field Strength Two-Dimensional Peptide Separations Using a Microfluidic Device

W. Hampton Henley and **J. Michael Ramsey**
The University of North Carolina at Chapel Hill, Department of Chemistry

Abstract

New instrumentation has been developed to improve the resolution, efficiency, and speed of microfluidic two-dimensional separations using micellar electrokinetic chromatography (MEKC) coupled to high field strength capillary electrophoresis (CE). Previously published two-dimensional separation instrumentation [1] from our group was limited to a maximum potential difference of 8.4 kV, resulting in an electric field strength of only ~200 V/cm in the first dimension. The circuit described in this report has been designed to couple a higher voltage supply with a rapidly switching, lower voltage supply to utilize the best features of each. Voltages applied in excess of 20 kV lead to high electric field strength separations in both dimensions, increasing the separation resolution, efficiency, and peak capacity while reducing the required analysis time. Detection rates as high as 6 peptides per second (based on total analysis time) were observed for a model protein tryptic digest separation. Additionally, higher applied voltages used in conjunction with microfluidic chips with longer length channels maintained higher electric field strengths and produced peak capacities of over 4,000 for some separations. Total separation time in these longer channel devices was comparable to that obtained in short channels at low field strength; however, resolving power improved approximately 3 fold.

Keywords

capillary electrophoresis; high electric field strength; microfluidic; peptides; two-dimensional separation

Introduction

The need for a high-speed peptide separation system with high peak capacity and resolving power has grown considerably due to increasing interest in protein and proteome analysis for potential medical applications and better understanding of protein function [2–5]. Complex biological samples can consist of many thousands of analytes and are therefore best analyzed by a separation system with high peak capacity. One commonly used approach is the coupling of two separation methods that are based upon fundamentally different separation mechanisms (orthogonal), as described by Giddings [6]. For truly orthogonal systems, the peak capacities of the two separations can be multiplied to obtain the peak capacity of the multidimensional separation. In systems were the separation mechanisms are somewhat related the peak capacity is relatively reduced [7] and can be evaluated based on conditional entropy [8]. Traditional two-dimensional (2-D) gel

J. Michael Ramsey, Goldby Distinguished Professor of Chemistry, Department of Chemistry, Chapman Hall, Rm 251, The University of North Carolina at Chapel Hill, Chapel Hill, NC 27599-3216, 919-962-7492 (office), 919-962-4952 (fax).

Conflict of interest statement
The authors are not aware of any financial or commercial conflict of interest regarding the research described herein.

separations such as isoelectric focusing/sodium dodecylsulfate-polyacrylamide gel electrophoresis (IEF/SDS-PAGE) provide 2-D results distributed in space across a slab gel. This technique can generate peak capacities from a few thousand to over ten thousand peaks, but traditional gels require extensive preparation and handling, relatively large amounts of sample, analyte staining after separation, and prolonged separation and analysis time (hours to days) [9–12].

Several approaches to small-scale multidimensional separations based on either column or capillary methods have been reported, although these methods suffer somewhat from the difficultly of coupling the two separations [10, 13–20]. Liquid phase 2-D separations typically use a 2-D in time strategy where the second dimension separation technique must be sufficiently rapid to allow multiple samplings of peaks eluting from the first dimension separation [13]. The advantages provided by microfluidic devices for implementing 2-D liquid phase separation strategies include low dead-volume coupling of the dimensions, small reagent and sample requirements, high separation efficiencies, and fast analysis times [21–29]. Previous work in our group demonstrated high peak capacity 2-D microfluidic separations of protein digests using MEKC coupled to CE [1]. In this approach, the sample was first separated in a long channel with a MEKC buffer that contained SDS. The analyte bands were then injected into short channel containing a buffer without SDS. The rapid dilution of the SDS in the band below its critical micelle concentration resulted in a fast CE-based separation. Although good results were reported with this system, hardware limitations of the high voltage instrumentation resulted in less than optimum MEKC and CE field strengths (200 and 2,400 V/cm respectively) that limited device performance. Additionally, the buffer used in these separations lacked the buffering capacity needed for multiple separations and may have contributed to poor long-term reproducibility.

MEKC has proven useful for neutral and charged analyte separations including peptides and proteins [30–35]. The peak capacity of a given micellar electrokinetic chromatographic separation is proportional to the square root of the separation efficiency:

$$n_c = 1 + \frac{\sqrt{N}}{4} \ln \frac{t_{mc}}{t_o} \quad (1)$$

where n_c is the peak capacity, N is the separation efficiency expressed as theoretical plates, t_{mc} is the micelle migration time, t_0 is the migration time required for unretained analytes [34]. The electroosmotic flow (EOF) velocity, the charged analytes' migration velocity, and the migration velocity of the micelles are all affected equally in magnitude by the electric field strength [31, 35]. Additionally, since the migration times (and hence the required separation analysis time) scale linearly with the inverse of the electric field strength, higher field strength will reduce the analysis time proportionately. As long as the degree of band broadening caused by Joule heating is small and the resistance to mass transfer between the aqueous and micellar phase is low, higher electric field strength should improve the efficiency of the separation linearly, and thus the peak capacity should improve as the square root of the increase in electric field strength [36–39].

Another approach to improving the peak capacity of a separation is to increase the distance that the analytes migrate under a given electric field strength. Increasing the migration distance in both dimensions should lead to an increase in peak capacity proportional to the product of the square root of the increase of the distance in each dimension [36]. The influence of the electric field strength on both the peak capacity and the migration time should translate to a greater number of detectable analytes per unit time as a function of increased electric field strength.

In this paper, novel high voltage instrumentation has been used to develop high field strength 2-D separations, particularly for the MEKC dimension. The impact of separation channel length was also explored at higher applied voltages. Observed improvements in peak capacity, resolution, and analysis time compare well to those predicted by theory.

Materials and methods

1. Reagents and Sample Preparation

5-Carboxytetramethylrhodamine, succinimidyl ester (5-TAMRA-SE) was purchased from Invitrogen Corporation (Carlsbad, CA). Bovine serum albumin (BSA), Tris base, and sodium dodecylsulfate (SDS) were purchased from Fisher Biotech. Boric acid was obtained from Mallinkrodt (Hazelwood, MO) and 1 N sodium hydroxide solution and 2-propanol Optima grade (IPA) were from Fisher Scientific. Trypsin (≥10,000 BAEE units/mg) and all other reagents were obtained from Sigma-Aldrich (St. Louis, MO),

The sample was prepared in a manner similar to that previously reported [1, 25]. A 10-mg/mL solution of BSA (1.98 mg total protein)) in 100 mM boric acid, pH = 8.4, was denatured at 80 °C for 1 hr. The whole solution was then mixed with 40 μL of 1 mg/mL aqueous trypsin solution and sonicated at 37 °C for 1 hr. A 140 μL aliquot of this solution was reacted with 0.7 mg of 5-TAMRA-SE dissolved in 70 μL DMSO for 4 hr. The solution was diluted 10-fold with 100 mM boric acid, pH=8.4. The labeled digest was stored at −20 °C until needed.

It was determined experimentally that the previously reported MEKC buffer used for 2-D separations in this chip geometry [1] (10 mM boric acid/20 mM SDS/10% IPA) lacked the buffering capacity required for reproducible or repeated analysis at high electric field strengths and extended separation times. The buffer chosen for the MEKC separation (first dimension) in this work was 150 mM Tris, 20 mM SDS, and 10% IPA with the pH adjusted to 9.4 with 0.1 N NaOH. The buffer for the CE separation (second dimension) was the same as the MEKC buffer, but contained no SDS. The IPA helps to lower the conductivity; it also commonly serves as an organic modifier for MEKC. Changes in pH caused by electrolysis were not sufficient to cause significant degradation in performance during the course of the separation, and problems with reproducibility between separations were not observed. As bands are injected from the MEKC dimension into the CE dimension, residual SDS is rapidly diluted below the critical micelle concentration and separates from the analyte bands giving a CE separation. Resistance measurements (Model 6487 Picoammeter/Voltage Source, Keithley Instruments, Inc., Cleveland, Ohio) taken from the microfluidic devices filled with these buffers showed that the channel conductivities are low and the currents are insufficient to cause significant Joule heating even at applied voltages up to 22 kV.

2. Microfluidic Devices

Microfluidic devices were fabricated from B270 glass substrates 100×100×0.9 mm^3 thick using standard photolithographic techniques as previously reported [40] Substrates precoated with 100 nm of chrome and 530 nm of positive AZ1500 photoresist were purchased from Telic (Valencia, CA). Chrome masks were designed using TurboCAD™ software, and fabricated by HTA Photomask (San Jose, CA). The mask design was transferred to the substrate using standard photolithography and the channels were etched using a 10:1 buffered oxide etch solution (Transene Company, Inc. Danvers, MA). Channel depths and widths were determined using a profilometer (KLA Tencor model P-15; San Jose, California). Chips were diced to 2.54 cm by 5.08 cm and access holes were drilled using an abrasive powder blaster (model MB1000, Comco, Inc., Burbank, CA). Chips were wet-bonded with a B270 cover slip and permanently fused by heat treatment at 550 °C for

10 hours. Cloning cylinders (6 mm, Fisher Scientific) were affixed to the chip using Norland 68 UV Optical Adhesive (Cranbury, NJ) to serve as fluid reservoirs.

Schematics of the chip designs used in this study are given in Figure 1. The rational for the serpentine channel design and the use of narrow, asymmetric tapered turns to reduce band broadening has been reported [1, 24, 41–43]. The design shown in Figure 1a is the same as that used in previous studies[1] and has an MEKC channel 19.6 cm in length and a CE channel 1.3 cm in length. The chip shown in Figure 1b is similar in design, but the channel lengths for both dimensions have been roughly doubled (37 cm and 2.3 cm, respectively), and the reservoirs have been carefully spaced to prevent high voltage arcing between those held at large potential differences. All channels on all devices were etched to a depth of ~10 μm. The chip in Figure 1a had an MEKC channel width at half depth of 70 μm and a CE channel width at half depth of 23 μm. The chip in Figure 1b had corresponding widths at half depth of 65 μm and 16 μm.

3. Microchip Operation and High Voltage Instrumentation

The operation of the microfluidic devices at low electric field strength was similar to that described by Ramsey et al [1]. Briefly, all channels were sequentially rinsed with 1 N NaOH solution and deionized water by filling the reservoirs with the solutions and then applying a vacuum first to reservoir SW2 and then reservoir S (Figure 1) for a minimum of 10 min. Reservoirs S, B1, and SW1 were then filled with MEKC buffer and B2, W, and SW1 with CE buffer by applying a vacuum to SW2 for 20 min. Buffer was removed from S and the sample (ten-fold diluted in MEKC buffer) was added.

Control of the fluid flow and separation voltages applied on the separation chip was accomplished using two high voltage power supplies, a Bertan (Hicksville, NY) model 2866A and a Spellman (Hauppauge, NY) model CZE1000PN30 REV F4 that were coupled together to exploit the best features of each supply. The Bertan supply consists of six independently controlled, programmable high voltage modules that output 0–10 kV at up to 100 μA. Each module is capable of rapidly switching potentials (~5 ms rise time) between two different states. The Spellman supply can output voltages between −30 kV to 30 kV at up to 300 μA, but the switching speed is relatively slow between transitions. Therefore, the Bertan supply was used for rapid, active switching of the reservoir potentials to control fluid flow and perform sample injections, while the Spellman was used to provide the higher voltages necessary to achieve high field strength separations.

The circuit used to couple the two high voltage supplies is shown in Figure 2. The shaded area of the circuit designates the microfluidic chip and points S, B1, SW1, B2, SW2, and W correspond to the chip reservoirs (compare to Figure 1). Points V1 and V2 represent junctions where the channels meet within the chip. The resistances shown for the channels on the chip are typical values obtained with the corresponding channels filled with MEKC and CE buffers. BHV1–6 denote the six outputs of the Bertan HV supply. D1–D3 are HV diodes (ED2139, Electronic Devices, Yonkers, NY) and D4–D7 are two ED2139 diodes in series. R1 represents the output resistance of the Spellman supply when it is not enabled. HVR 1–3 are high voltage relays (Kilovac model K81C245, Santa Barbara, CA) that switch between the first 3 outputs of the Bertan supply and ground.

Fluid flow on the chip was based upon a “gated” injection format [44]. At the beginning of an experiment, the Spellman supply is not enabled, and relays HVR1–3 are positioned as shown in Figure 2. In a typical experiment, potentials of 8, 8.4, 6.4, 4.8, 1.2, and 0 kV are applied using BHV 1–6 respectively for 5 min to establish the closed gates at V1 and V2. Diodes D4–7 are forward-biased, and diodes D1–3 are reverse-biased. To perform the injection, 8, 7.4, 6.8, 4.8, 1.2, and 0 kV are applied using BHV 1–6 respectively. R2 and R5

allow a small amount of current from the sample reservoir to flow into B1 and SW1, and the current sinking ability of power supplies BHV5 and BHV6 allow current to flow into the MEKC channel, injecting a small amount of sample over the span of a few seconds. The outputs of the Bertan supply are switched back to 8, 8.4, 6.4, 4.8, 1.2, and 0 kV for 5 seconds to close the gate and allow the analyte band to migrate a short distance. At this point, relays HVR1–3 are switched to ground, the outputs of BHV1–3 are lowered to ground, and the Spellman supply is enabled. The HV output of the Spellman supply (from 10–30 kV) causes diodes D1–3 to be forward-biased, and diodes D4–6 to be reverse-biased. The full voltage output of the Spellman supply is applied to B1, and the voltage divider composed of resistors R3–5 insures the proper biasing of the MEKC reservoirs to maintain a closed gate.

After the Spellman supply has been enabled, the voltages at S, B1, and SW1 are held at separation voltages and injections of analytes migrating out the MEKC channel can be made into the CE channel. To make these injections, the voltage applied to reservoir B2 is decreased (for example from 4.8 kV to 1.4 kV for 20 ms every 1 s) so that buffer flow from the reservoir decreases and allows a plug of MEKC buffer to enter the CE channel. Current is always sourced from B2, and so a high voltage blocking diode, D7, can be used to protect BHV4 in the event of HV flashover from one of the three MEKC reservoirs held at a much higher potential. D7 remains forward-biased as the potential from BHV4 is always higher than the potential at point V2. For proper operation of the chip, SW2 and W must always sink current, preventing the use of a protection diode for BHV5–6. Instead, a 2,200 V avalanche diode between BHV5 and ground is used to provide protection for the Bertan output at SW2 in the event of a HV flashover from another reservoir, and BHV6 is tied directly to ground. For added protection against high voltage arcing, the electrodes were fitted with Pyrex tubes that slipped over the chip reservoirs and extended several centimeters above the chip. This arrangement increased the effective pathlength between each reservoir so that higher separation potentials could be used. Actual potentials and timing used for the separations discussed in this work are given in Table 1.

The high voltage power supplies were controlled by a National Instruments PCI-6713 DAQ card and data collection was performed using a National Instruments PCI-6251 DAQ card. An IBM MT-M 8141-UN5 computer with software written in-house using LabVIEW™ version 8 (National Instruments Corporation, Austin, TX) controlled the cards and recorded the data.

4. Laser-induced Fluorescence Detection and Data Processing

Peptides labeled with 5-TAMRA were detected using laser-induced fluorescence. The beam from a Coherent, Inc. (Santa Clara, CA) Innova 300 FReD Ar ion laser tuned to 514.5 nm, 100 mW output was passed through a neutral density filter to reduce its power to 10 mW. After passing through a line filter (514.5DF10, Omega Optical, Inc., Brattleboro, VT) the beam was reflected by a dichroic filter (model XF2030 525DRLP, Omega Optical). A 40X long-working-distance objective (CD-240-M40, Creative Devices, Neshanic Station, NJ) was used to focus the beam onto the chip at the detection point. The same objective was used to collect the fluorescence, which passed through the dichroic filter and was spatially filtered with a 1-mm pinhole (Melles Griot, Carlsbad, CA). The fluorescence was spectrally filtered using a Razor Edge Raman Filter 514.5 nm (LPO1-514RS-25, Semrock) and an emission filter (580DF30, Omega Optical) before it was detected by a photon multiplier tube (H7732-10, Hamamatsu Photonics K.K. Bridgewater, NJ). Current from the PMT was collected and amplified using a Stanford Research Systems, Inc. (Sunnyvale, CA) model SR570 low current preamplifier.

Data were collected as a linear trace and subsequently divided into a series of CE injection and runs using software written in LabVIEW™ version 8. Frequency filtering was employed to remove line (60 Hz) and other nonrandom noise. The data were plotted as an image plot with the intensity of the LIF signal determining the degree of contrast for each pixel [1, 27]. Each MEKC band was sampled by several CE separations, resulting in an image plot closely resembling that of a 2-D gel separation.

Peak capacities reported here were calculated for each individual sample. The separation window of each dimension was determined by subtracting the migration time of the first analyte peak from that of the last analyte peak. In the interest of keeping the total analysis time small, the bands from MEKC dimension were injected into the CE dimension at a fast rate. In some cases, the time between injections was smaller than the actual CE separation window, i.e., overlapping injections. The separation widow (or the time between injections, whichever was smaller) was divided by the average width of the predominant analyte peaks to obtain the capacity of each dimension. The capacity of the first dimension was then multiplied by that of the second dimension to determine the overall capacity for each separation.

Results and Discussion

The data shown in Table 2 and the 2-D plots shown in Figure 3 demonstrate the improved resolution and peak capacity achieved using this instrumentation. Separation A was conducted using the higher buffering capacity buffer with the relatively low field strength in the shorter channel chip (Figure 1a) previously reported [1]. Separation B used the same buffer and chip design, but much higher applied voltages. The conditions used for B were optimized for speed and sensitivity. The higher current in the MEKC dimension caused relatively large volumes of material to be injected into the CE dimension, improving sensitivity. The duration of the gated injection was reduced to only 15 ms to limit band broadening. Separation C was conducted in the longer channel chip, Figure 1b, at high applied voltages. This separation was optimized for high resolution. The MEKC bands were sampled every 1.5 s to decrease the total analysis time, although some bands were detected outside this window.

The improvements in peak capacity observed in both dimensions broadly follow the expected trends. Although both separations A and B were performed using the same buffer system and on the same microfluidic chip, the electric field strength in the MEKC dimension for separation B (650 V/cm) is more than threefold higher than that for separation A. Based on the increased field strength, a √3 improvement would be expected in this dimension. The peak capacity for the MEKC dimension for separation B is 95, or almost exactly √3 times higher than the peak capacity for the MEKC dimension of separation A (54). The CE field strength is 1.4-fold higher in separation B, and the peak capacity has improved by a factor close to 1.2, as expected from theory. These results indicate that sources of band broadening including the resistance to mass transfer between the aqueous and micellar phases and Joule heating are relatively small under these conditions. Improved sensitivity is also seen as more material was injected from the MEKC dimension into the CE dimension under these conditions.

Another benefit of increased electric field strength used in separation B is the reduced analysis time. The greater than threefold increase in electric field strength in the first dimension of separation B reduces the analysis time to slightly less than one third that required for separation A. The greater peak capacity and shorter analysis time translates into an ~ 7.7-fold increase in the analysis rate (analytes/s) when compared to separation A.

The higher peak capacity achieved in separation C relative to separation A is due to resolution improvements from a combination of longer separation channels and higher electric fields. Although the separation channels are almost twice as long in separation C as in separation A, the higher electric field strength produced from the higher applied voltages results in an analysis time only ~70% longer. The higher peak capacity (~4-fold) of this separation combined with the comparable analysis time results in a higher number of analyte peaks that can be detected in a given analysis time (2.1 as compared to 0.78 analytes/s).

The calculated peak capacity of the CE dimension of separation C is only slightly better than that of separation B possibly due to several factors. The high rate at which bands from the MEKC dimension were sampled reduced the effective separation window below that which was actually observed. The CE electric field strength was also slightly lower than that used for separation B. Differences in the conditions used to sample the bands from the MEKC dimension may also have affected the rate at which the SDS was separated from the sample plug, potentially leading to increase band broadening. Future work will explore further optimization of the chip geometry and buffer composition to obtain greater resolving power in both dimensions and thus higher peak capacities and analysis rates (peaks/s).

Concluding remarks

The use of higher applied voltages for microfluidic two-dimensional separations offers the potential for extremely fast, high resolution, and high peak capacity separations of peptides and protein digests. The peak capacity gained by the implementation of higher voltage instrumentation for higher electric fields is ultimately limited by electrical arcing between the reservoirs or Joule heating. The channel geometry and bulk material properties of microfluidic devices minimize Joule heating and its effects [45], and the appropriate reservoir spacing and the use of dielectric materials to provide insulation can easily eliminate high voltage arcing or corona at voltages ≤30 kV while maintaining a small microfluidic footprint.

Acknowledgments

The authors thank John Peterson of the UNC Chemistry Electronics Facility for helpful discussions concerning the high voltage instrumentation, Kevin Braun for development of the 2-D image processing software, and J.P. Alarie for help with instrumentation. Funding was provided by the National Heart, Lung, and Blood Institute (NHLBI) grant N01-HV-28182.

List of abbreviations

IPA	2-propanol
5-TAMRA-SE	5-Carboxytetramethylrhodamine, Succinimidyl Ester

References

1. Ramsey JD, Jacobson SC, Culbertson CT, Ramsey JM. Anal. Chem. 2003; 75:3758–3764. [PubMed: 14572041]
2. Azad NS, Rasool N, Annunziata CM, Minasian L, Whiteley G, Kohn EC. Mol. Cell. Proteomics. 2006; 5:1819–1829. [PubMed: 16737951]
3. Goodlett DR. Proteomics of Neurodegenerative Disease. 2006:1–23.
4. Ye M, Jiang X, Feng S, Tian R, Zou H. TrAC, Trends Anal. Chem. 2007; 26:80–84.
5. Palcy S, Chevet E. Proteomics. 2006; 6:5467–5480. [PubMed: 17044000]
6. Giddings JC. Anal. Chem. 1984; 56:1258A–1260A. 1262A, 1264A, 1266A, 1268A, 1270A.
7. François I, Sandra K, Sandra P. Anal. Chim. Acta. 2009; 641:14–31. [PubMed: 19393362]

8. Pourhaghighi MR, Karzand M, Girault HH. Anal. Chem. 2011; 83:7676–7681. [PubMed: 21913671]
9. O'Farrell PH. J. Biol. Chem. 1975; 250:4007–4021. [PubMed: 236308]
10. Hille JM, Freed AL, Watzig H. Electrophoresis. 2001; 22:4035–4052. [PubMed: 11824628]
11. Lilley KS, Razzaq A, Dupree P. Curr. Opin. Chem. Biol. 2002; 6:46–50. [PubMed: 11827822]
12. Gorg A, Obermaier C, Boguth G, Harder A, Scheibe B, Wildgruber R, Weiss W. Electrophoresis. 2000; 21:1037–1053. [PubMed: 10786879]
13. Bushey MM, Jorgenson JW. Anal. Chem. 1990; 62:161–167. [PubMed: 2310013]
14. Holland LA, Jorgenson JW. Anal. Chem. 1995; 67:3275–3283. [PubMed: 8686888]
15. Hooker TF, Jorgenson JW. Anal. Chem. 1997; 69:4134–4142.
16. Moore AW Jr, Jorgenson JW. Anal. Chem. 1995; 67:3448–3455. [PubMed: 8686893]
17. Moore AW Jr, Jorgenson JW. Anal. Chem. 1995; 67:3456–3463. [PubMed: 8686894]
18. Opiteck GJ, Jorgenson JW, Anderegg RJ. Anal. Chem. 1997; 69:2283–2291. [PubMed: 9212702]
19. Opiteck GJ, Lewis KC, Jorgenson JW, Anderegg RJ. Anal. Chem. 1997; 69:1518–1524. [PubMed: 9109352]
20. Michels DA, Hu S, Schoenherr RM, Eggertson MJ, Dovichi NJ. Mol. Cell. Proteomics. 2002; 1:69–74. [PubMed: 12096142]
21. Reyes DR, Iossifidis D, Auroux P-A, Manz A. Anal. Chem. 2002; 74:2623–2636. [PubMed: 12090653]
22. Auroux P-A, Iossifidis D, Reyes DR, Manz A. Anal. Chem. 2002; 74:2637–2652. [PubMed: 12090654]
23. Buch JS, Rosenberger F, Highsmith WE Jr, Kimball C, DeVoe DL, Lee CS. Lab Chip. 2005; 5:392–400. [PubMed: 15791336]
24. Culbertson CT, Jacobson SC, Ramsey JM. Anal. Chem. 2000; 72:5814–5819. [PubMed: 11128941]
25. Gottschlich N, Jacobson SC, Culbertson CT, Ramsey JM. Anal. Chem. 2001; 73:2669–2674. [PubMed: 11403315]
26. Li Y, Buch JS, Rosenberger F, DeVoe DL, Lee CS. Anal. Chem. 2004; 76:742–748. [PubMed: 14750871]
27. Rocklin RD, Ramsey RS, Ramsey JM. Anal. Chem. 2000; 72:5244–5249. [PubMed: 11080871]
28. Shadpour H, Soper SA. Anal. Chem. 2006; 78:3519–3527. [PubMed: 16737203]
29. Wang Y-C, Choi MH, Han J. Anal. Chem. 2004; 76:4426–4431. [PubMed: 15283583]
30. Ferguson PD, Goodall DM, Loran JS. Anal. Chem. 1998; 70:4054–4062. [PubMed: 21651241]
31. Foley JP. Anal. Chem. 1990; 62:1302–1308.
32. Iadarola P, Cetta G, Luisetti M, Annovazzi L, Casado B, Baraniuk J, Zanone C, Viglio S. Electrophoresis. 2005; 26:752–766. [PubMed: 15669008]
33. Molina M, Silva M. Electrophoresis. 2002; 23:3907–3921. [PubMed: 12481284]
34. Nielson, KR.; Foley, JP. Capillary Electrophoresis: Theory and Practice. Camilleri, P., editor. Boca Raton: CRC Press; 1998. p. 135-182.
35. Terabe S, Otsuka K, Ichikawa K, Tsuchiya A, Ando T. Anal. Chem. 1984; 56:111–113.
36. Hutterer KM, Birrell H, Camilleri P, Jorgenson JW. J. Chromatogr. B. Biomed. Sci. App. 2000; 745:365–372.
37. Terabe S, Otsuka K, Ando T. Anal. Chem. 1989; 61:251–260.
38. Sepaniak MJ, Cole RO. Anal. Chem. 1987; 59:472–476.
39. Qi S, Tian K, Zhang H, Chen X. Anal. Lett. 2006; 39:2039–2053.
40. Jacobson SC, Hergenroder R, Koutny LB, Warmack RJ, Ramsey JM. Anal. Chem. 1994; 66:1107–1113.
41. Molho JI, Herr AE, Mosier BP, Santiago JG, Kenny TW, Brennen RA, Gordon GB, Mohammadi B. Anal. Chem. 2001; 73:1350–1360.
42. Paegel BM, Hutt LD, Simpson PC, Mathies RA. Anal. Chem. 2000; 72:3030–3037. [PubMed: 10939363]

43. Griffiths SK, Nilson RH. Anal. Chem. 2001; 73:272–278. [PubMed: 11199977]
44. Jacobson SC, Koutny LB, Hergenroeder R, Moore AW Jr, Ramsey JM. Anal. Chem. 1994; 66:3472–3476.
45. Jacobson SC, Culbertson CT, Daler JE, Ramsey JM. Anal. Chem. 1998; 70:3476–3480.

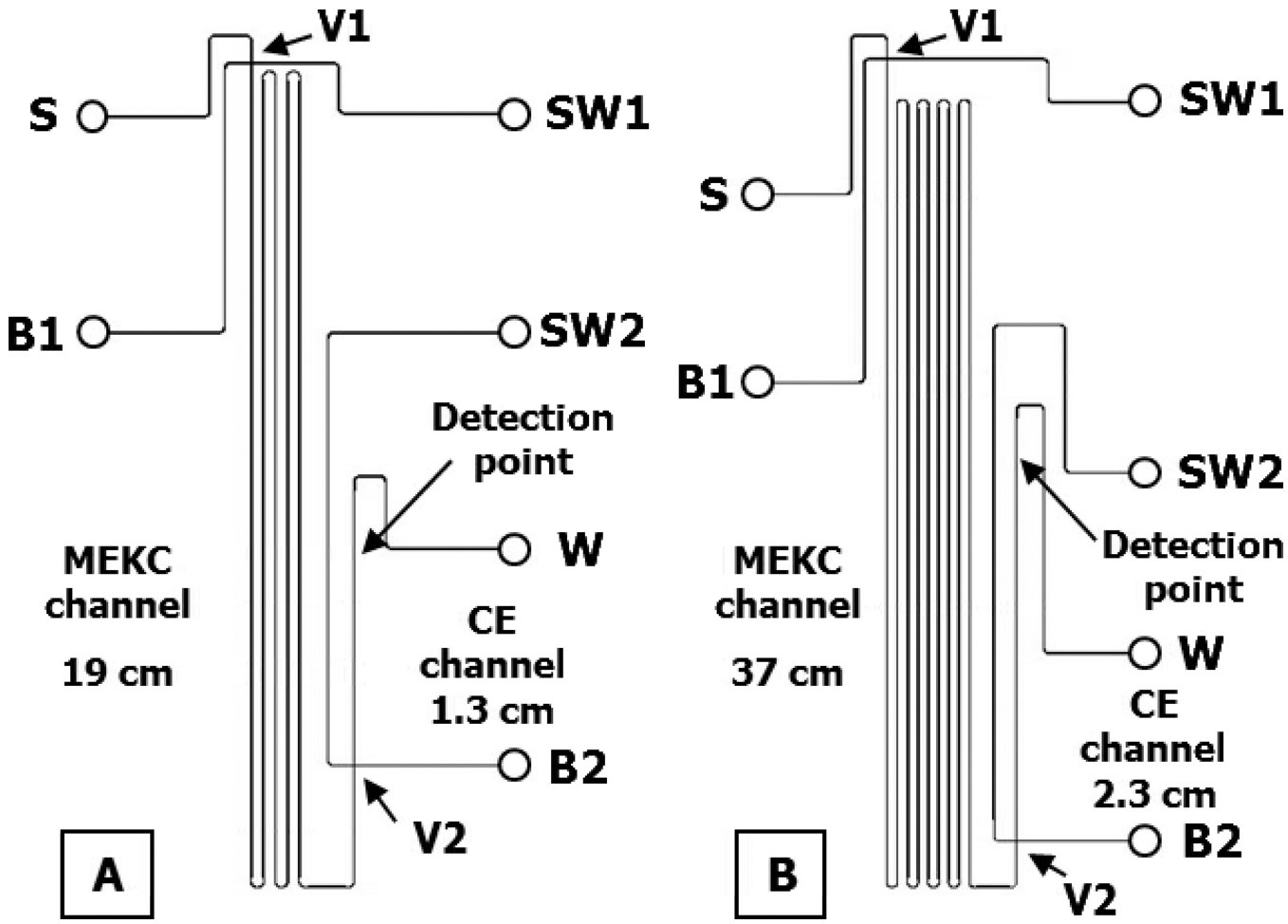

Figure 1.

Layout and design of the two-dimensional separation chips are shown. A) The short channel design for fast separations has a 19.6 cm MEKC channel and a 1.3 cm CE channel. B) The longer channel design has a 37 cm MEKC channel and a 2.3 cm CE channel for high resolution and high peak capacity separations. S=sample; B1=MEKC buffer; SW1=sample waste 1; B2=CE buffer; SW2=sample waste 2; W=waste.

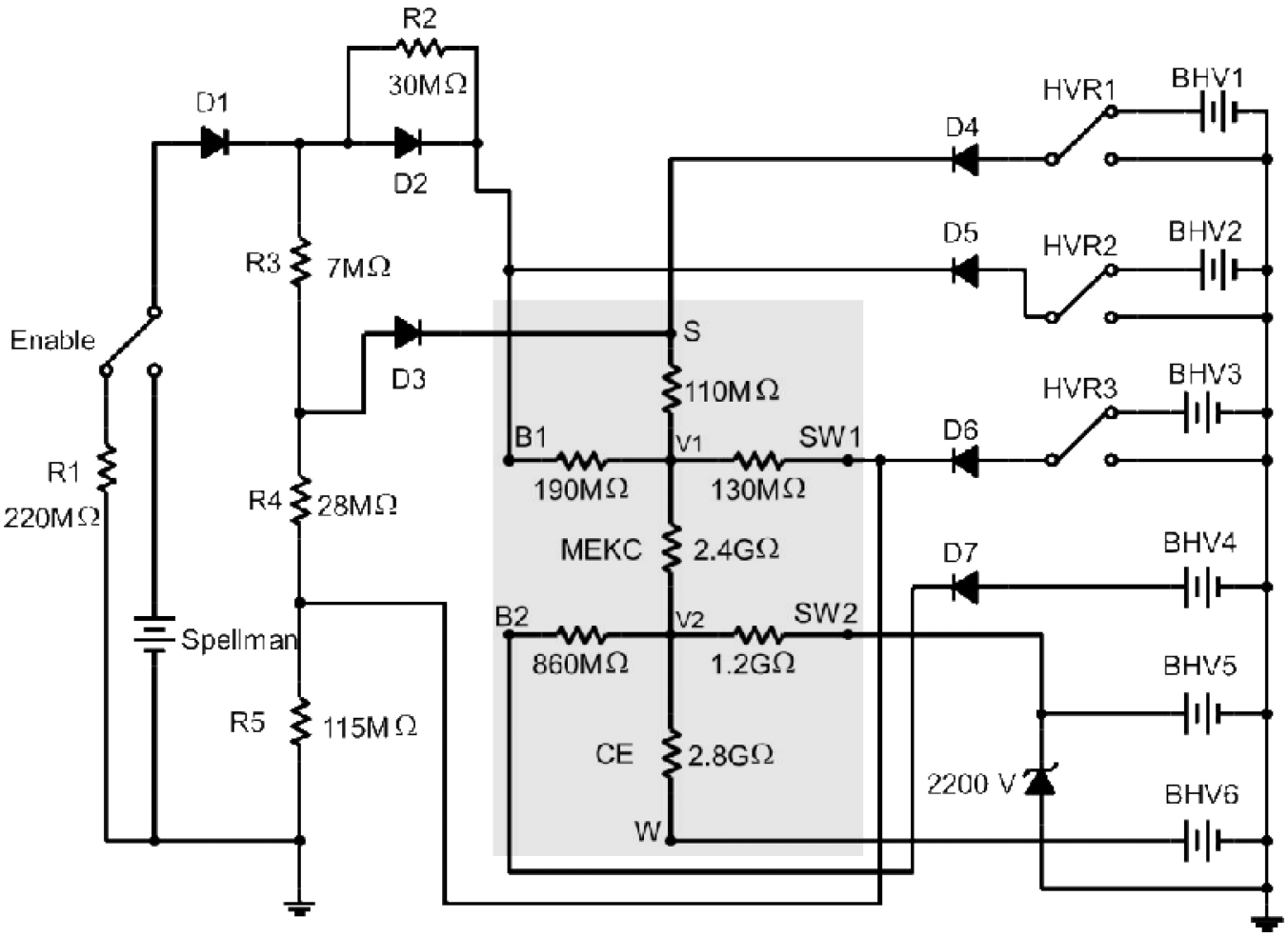

Figure 2.

Design schematic of high voltage instrumentation coupling the two power supplies used for high electric field strength 2-D separations is shown. The shaded region shows the equivalent circuit for a typical separation. D1–D7 are high voltage blocking diodes, R3–R5 form a voltage divider to bias the MEKC reservoirs. BHV1–6 are the individual outputs from the Bertan power supply. HVR1–3 are high voltage relays used to switch between BHV1–3 and ground.

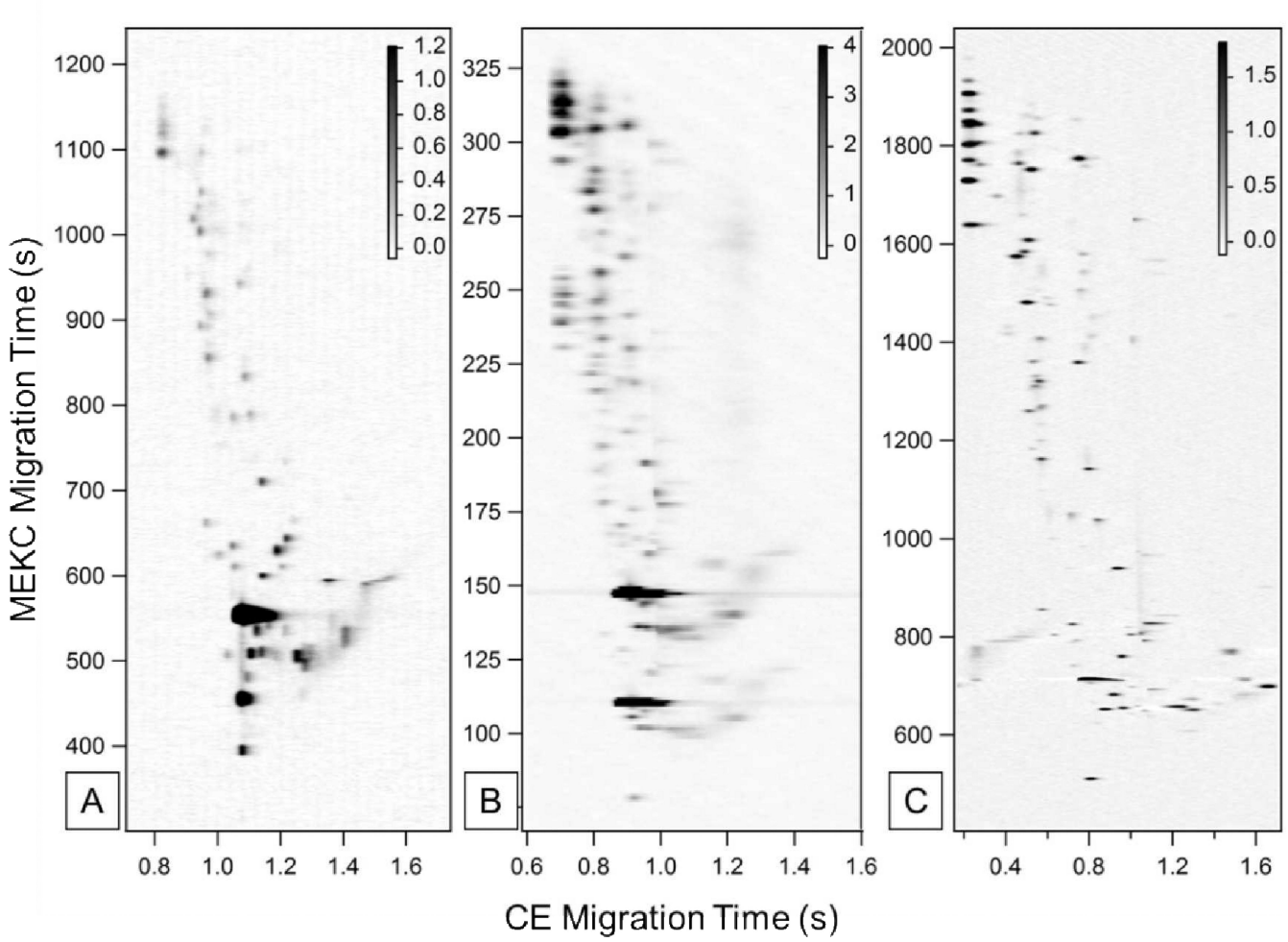

Figure 3.

Separation of 5-TAMRA-SE labeled BSA tryptic digest using the same MEKC and CE buffers shown as 2-D grayscale images. A) A separation at standard voltages using the chip design of Figure 1A. B) The same sample separated using higher applied voltages and shorter CE injection times using chip design of Figure 1A. Higher current from the MEKC channel resulted in more sample injected from the MEKC band into the CE dimension, increasing sensitivity. C) Chip design shown in Figure 1B with roughly twice the channel length in each dimension was used at electric field strengths higher than those used in A by applying higher potentials in both dimensions. A 100-point median filter baseline subtraction was used to remove long-term baseline drift from plot C. Relative signal intensity is given by the scale bar in the upper right-hand corner of each plot.

Table 1

Timing (s) and applied voltage (kV) profiles for the three separations are shown in this table. After completion of the first cycle, the software cycles between “Separation” or “HV Separation” and “CE injection” values until the separation is complete (up to 3000 s).

Separation A	**Time (s)**	**S**	**B1**	**SW1**	**B2**	**SW2**	**W**
Establish Gates	300	8	8.4	6.4	4.8	1.2	0
MEKC injection	10	8	7.4	6.8	4.8	1.2	0
Separation	1	8	8.4	6.4	4.8	1.2	0
CE injection	0.04	8	8.4	6.4	1.4	1.2	0
Separation B	**Time (s)**	**S**	**B1**	**SW1**	**B2**	**SW2**	**W**
Establish Gates	300	8	8.4	6.4	4.8	1.2	0
MEKC injection	10	8	7.4	6.8	4.8	1.2	0
Separation	5	8	8.4	6.4	4.8	1.2	0
HV Separation	1	19	20	15.2	4.8	1.2	0
CE injection	0.015	19	20	15.2	1.4	1.2	0
Separation C	**Time (s)**	**S**	**B1**	**SW1**	**B2**	**SW2**	**W**
Establish Gates	300	8	8.4	6.4	4.8	1.2	0
MEKC injection	7	8	7.4	6.8	4.8	1.2	0
Separation	5	8	8.4	6.4	4.8	1.2	0
HV Separation	1.5	21	22	16.8	8	5	0
CE injection	0.04	21	22	16.8	1.4	1.2	0

Table 2

Comparison of the properties of two-dimensional separations under three different operating conditions, showing improvements in peak capacity and the number of analytes detected at higher electric field strengths.

	Separation A	Separation B	Separation C
MEKC channel length (cm)	19.6	19.6	37
CE channel length (cm)	1.3	1.3	2.3
Highest potential applied (kV)	8.4	20	22
MEKC field strength (V/cm)	210	650	340
CE field strength (V/cm)	2600	3700	3200
MEKC/CE average peak width (s)	15.8 / 0.052	2.75 / 0.044	7.7 / 0.072
MEKC/CE separation window (s)	838 / 0.9	265 / 0.9	1500 / 1.5
Peak Capacity MEKC / CE	54 / 17	95 / 20.5	195 / 21
Peak Capacity (Total)	920	1950	4100
Analytes/total analysis time	0.78	6.0	2.1
Analyte spots detected	~65	~95	~95